or subsequent (possibly parent body) processing is indicated.

References and Notes

1. H. C. Urey, *Proc. Natl. Acad. Sci. U.S.A.* **41**, 127 (1955).
2. M. Wadhwa, S. S. Russell, in *Protostars and Planets IV*, V. Mannings *et al.*, Eds. (University of Arizona Press, Tucson, AZ, 2000), pp. 995–1018.
3. T. Lee, D. A. Papanastassiou, *Geophys. Res. Lett.* **1**, 225 (1974).
4. Y. Amelin, A. N. Krot, I. D. Hutcheon, A. A. Ulyanov, *Science* **297**, 1678 (2002).
5. G. J. MacPherson, A. M. Davis, E. K. Zinner, *Meteoritics* **30**, 365 (1995).
6. S. S. Russell, G. Srinivasan, G. R. Huss, G. J. Wasserburg, G. J. MacPherson, *Science* **273**, 757 (1996).
7. M. Bizzarro, J. A. Baker, H. Haack, *Nature* **431**, 275 (2004).
8. A. Galy, E. D. Young, R. D. Ash, R. K. O'Nions, *Science* **290**, 1751 (2000).
9. E. D. Young, R. D. Ash, A. Galy, N. S. Belshaw, *Geochim. Cosmochim. Acta* **66**, 683 (2002).
10. A. Galy, I. D. Hutcheon, J. N. Grossman, Lunar and Planetary Science Conference XXXV, 15 to 19 March 2004, Houston (Lunar and Planetary Institute, Houston, TX, 2004).
11. Materials and methods are available as supporting materials on *Science* Online.
12. K. I. Mahon, *Int. Geol. Rev.* **38**, 293 (1996).
13. F. A. Podosek *et al.*, *Geochim. Cosmochim. Acta* **55**, 1083 (1991).
14. T. LaTourrette, I. D. Hutcheon, Lunar and Planetary Science Conference XXX, 15 to 19 March 1999, Houston (Lunar and Planetary Institute, Houston, TX, 1999).
15. T. LaTourrette, G. J. Wasserburg, *Earth Planet. Sci. Lett.* **158**, 91 (1998).
16. O. Lovera, F. M. Richter, M. H. Harrison, *J. Geophys. Res.* **94**, 17017 (1989).
17. J. P. Greenwood, Lunar and Planetary Science Conference XXXV, 15 to 19 March 2004, Houston (Lunar and Planetary Institute, Houston, TX, 2004).
18. E. M. Stolper, *Geochim. Cosmochim. Acta* **46**, 2159 (1982).
19. For example, in a CAI the same size as E44 but with anorthite/(anorthite + melilite) = 0.05 rather than 0.25, the anorthite + melilite system would be reset when reaction progress variable = 0.4×10^{-3}, corresponding to 10 years at 1600 K or 10^7 years at 900 K.
20. H. Y. McSween, A. Ghosh, R. E. Grimm, L. Wilson, E. D. Young, in *Asteroids III*, W. Bottke *et al.*, Eds. (University of Arizona, Tucson, AZ, 2003), pp. 559–571.
21. K. Keil, *Planet. Space Sci.* **48**, 887 (2000).
22. S. J. Weidenschilling, *Icarus* **165**, 438 (2003).
23. F. H. Shu, H. Shang, T. Lee, *Science* **271**, 1545 (1996).
24. F. H. Shu, H. Shang, M. Gounelle, A. F. Glassgold, T. Lee, *Astrophys. J.* **548**, 1029 (2001).
25. S. J. Desch, H. C. Connolly, *Meteorit. Planet. Sci.* **37**, 183 (2002).
26. J. A. Wood, *Meteorit. Planet. Sci.* **31**, 641 (1996).
27. G. J. MacPherson, A. M. Davis, *Geochim. Cosmochim. Acta* **57**, 231 (1993).

28. The authors wish to thank A. Krot for providing sample E44. The work was supported by grants from the NASA Cosmochemistry program, the NASA Astrobiology Institute, the Particle Physics and Astronomy Research Council (UK), and the National Science Foundation (USA).

Supporting Online Material

www.sciencemag.org/cgi/content/full/1108140/DC1
Materials and Methods
SOM Text
Figs. S1 to S8
Table S1
References

1 December 2004; accepted 11 February 2005
Published online 3 March 2005;
10.1126/science.1108140
Include this information when citing this paper.

Structure of a γδ T Cell Receptor in Complex with the Nonclassical MHC T22

Erin J. Adams,[1,2,3] Yueh-Hsiu Chien,[1,3] K. Christopher Garcia[1,2,3]*

γδ T cell receptors (TCRs), αβ TCRs, and antibodies are the three lineages of somatically recombined antigen receptors. The structural basis for ligand recognition is well defined for αβ TCR and antibodies but is lacking for γδ TCRs. We present the 3.4 Å structure of the murine γδ TCR G8 bound to its major histocompatibility complex (MHC) class Ib ligand, T22. G8 predominantly uses germline-encoded residues of its δ chain complementarity-determining region 3 (CDR3) loop to bind T22 in an orientation substantially different from that seen in αβ TCR/peptide-MHC. That junctionally encoded G8 residues play an ancillary role in binding suggests a fusion of innate and adaptive recognition strategies.

γδ T cells, like αβ T cells and B cells, generate a diverse repertoire of antigen-recognition receptors through somatic rearrangement of V, D, and J gene segments. This process generates a heterodimeric receptor composed of two chains, each encoding a variable (V) and constant (C) domain. It has been convincingly demonstrated that αβ and γδ T cells have different functional roles in the immune system (*1*), yet the identity of endogenous ligands for γδ T cells is unclear and little is known about the molecular basis of ligand recognition through their specific γδ TCRs. From the few defined γδ TCR ligands, it is apparent that γδ TCRs recognize a diverse array of antigens and that, like antibodies, they appear to recognize these antigens directly, distinguishing them from αβ TCRs that require antigen presentation by MHC [reviewed in (*2*)].

Early immunogenetic studies of αβ TCR and antibodies gave strong clues into the structural properties by which they would recognize ligand (*3*). In αβ TCR there is a concentration of diversity in the CDR3 (10^{15} unique junctions), relative to germline-encoded CDR1 and CDR2 derived from V-domain pairing (2500 pairs). In contrast, antibodies exhibit less CDR3 junctional diversity (10^{11} unique junctions) relative to the germline-encoded diversity of their CDR1 and CDR2 loops (90,000 pairs). Consistent with this, structural studies showed that the αβ TCR CDR3 primarily contact antigenic peptide, while CDR1 and CDR2 loops contact conserved helical portions of the MHC surface (*4*). Antibodies, although predominantly using CDR3, also make substantial use of CDR1 and CDR2 in recognizing a diverse antigenic repertoire.

A similar analysis of the γδ TCR repertoire indicates that they have the highest potential CDR3 diversity (10^{18}) but limited diversity conferred by pairing of germline-encoded V domains, with only ~7 Vγs and ~10 Vδs in the mouse (70 potential pairs) (*3*, *5*). CDR3 length distribution in γδ TCRs is more similar to antibodies than to αβ TCRs in that the CDR3δ loops are long and variable, and the CDR3γ loops are short and constrained (*5*). Given the long and potentially diverse CDR3δ of γδ TCR, it would seem likely that this loop is used directly for antigen recognition. However, many infection models involving γδ T cells show restricted V-gene usage (*6*), which suggests that γδ TCR specificity is determined by germline-derived V domains alone.

We have determined a 3.4 Å crystal structure of the γδ TCR G8 in complex with the nonclassical MHC Ib protein T22 (*7*, *8*). The G8 γδ heterodimer binds protein products of the T22 and T10 loci (95% homology), as do 0.09 to 0.6% of γδ T cells in the spleen and intraepithelial lymphocytes (IELs) of unstimulated mice (*9*, *10*). Both T22 and T10 have a canonical class I fold, except that the C terminus of the α2 helix is unraveled, disrupting the peptide-binding groove and exposing the underlying β-sheet platform (*11*, *12*). Binding measurements with refolded T22 (*9*) and the lack of a bound ligand in the structures of T10 (*12*) and T22 (*11*) confirm that G8 recognition of T10/T22 is direct and not dependent on antigen processing. The structure shows that the CDR loops, predominantly germline-encoded residues of the junctionally recombined CDR3δ, are directly used in γδ TCR recognition of an MHC ligand, resulting in a binding mode distinct from either antibody/antigen or αβ TCR/pMHC interactions.

Expression and structure determination of the γδ TCR and its ligand. The soluble G8 γδ TCR and its MHC ligand, T22, were expressed from baculovirus-infected insect cells, which produced a glycosylated G8 γδ TCR containing the canonical interchain di-

[1]Department of Microbiology and Immunology, [2]Department of Structural Biology, [3]Program in Immunology, Stanford University School of Medicine, Fairchild D319, 299 Campus Drive, Stanford, CA 94035–5124, USA.

*To whom correspondence should be addressed. E-mail: kcgarcia@stanford.edu

sulfide (*13*). We confirmed binding of G8 to T22 by native gel shift and surface plasmon resonance (SPR). We crystallized the G8/T22 complex, collected a complete x-ray data set (Table 1), and determined a molecular replacement solution using the human γδ TCR G115 (*14*) and the unliganded structure of T22 (*11*) as search models. We subsequently refined the complex structure to 3.4 Å resolution (Table 1). There are two complexes in the asymmetric unit, forming a dimer along a Vδ interface (fig. S1). The Cγ and Cδ domains of one G8 γδ TCR (complex #2) exhibited partial disorder, and the electron-density map for these domains was poor, as reflected in elevated B values (Table 1) (*13*). All other parts of the structure are well resolved. The TCRs in the two respective complexes show a slight difference in orientation due to movement around a pivot point formed by the contact patch between CDR3δ and T22. This shift results in some minor variations in contact between the CDR1δ, CDR2δ, HV4δ, and CDR3γ loops and T22 between the two complexes. Because the individual components in the two complexes are identical to within the limits of our resolution [root mean square deviations (RMSD) of Cα individual G8 V domains and T22/β_2m are each 0.9 Å], we discuss complex #1 below and separately discuss the pivot and its implications in a later section.

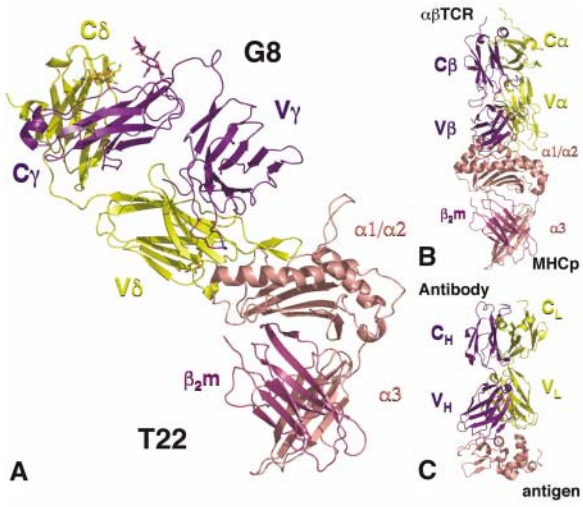

Fig. 1. Structure of the G8/T22 complex and comparison with ligand-recognition modes seen in αβTCR/pMHC and antibody/antigen complexes. (**A**) Ribbon diagram showing the overall backbone structure of the G8/T22 complex (only one of the two complexes in the asymmetric unit of the crystal is shown). The G8 γδTCR is shown in purple (γ chain) and yellow (δ chain), and T22 is shown in salmon (heavy chain) and magenta (β_2m). G8 binds T22 at a tilted angle, with an extended CDR3 loop from the δ chain forming extensive contact with T22's β-sheet platform and α1 helix. (**B**) The 2C αβTCR (α chain shown in yellow, β chain in purple) complexed with H2-K^b-dEV8 (heavy chain in salmon, β_2m in fuschia) (*25*). (**C**) Structure of the complex between the Fab of antibody HyHEL (heavy chain in purple, light chain in yellow) and hen egg-white lysozyme (shown in salmon) (*32*). All figures were produced with the Pymol software (*33*).

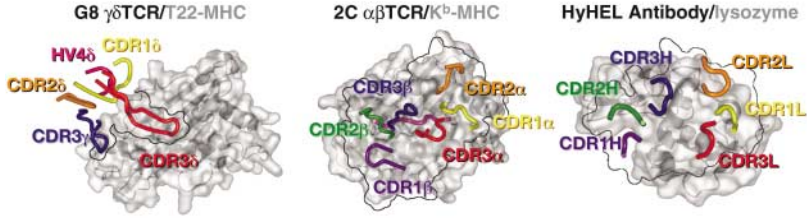

Fig. 2. Recognition footprints and location of CDR loops for γδTCR/MHC Ib, αβTCR/peptide-MHC, and an antibody/lysozyme complex. (**Left**) The CDR1δ (yellow), CDR2δ (orange), CDR3δ (red), HV4δ (hot pink), and CDR3γ (blue) loops of the G8 γδTCR are superimposed on a molecular surface of T22, with the ribbon backbone visible through the transparent surface. The remaining CDR loops of G8 do not participate in binding and therefore are not shown. The footprint of the G8 γδ TCR on T22 is shown as a black outline and occludes only a small portion of the T22 platform in comparison with that seen in αβTCR/pMHC (**middle**) (*25*) and antibody/antigen (**right**) (*32*). The black outlines of the three antigen receptors were traced around the perimeters of the respective molecular surfaces.

Table 1. Crystallographic statistics.

Data collection	
Space group	$P2_12_12_1$
Unit cell (Å) (a, b, c)	110.53, 113.05, 167.97
Source	ALS, 8.2.1
Resolution (Å) (last shell)	20–3.4 (3.52–3.40)
Unique reflections	28,542
Redundancy	5.9 (3.1)
Completeness (%)	96.9 (88.4)
I/σ (I)	23.9 (2.6)
R_{merge} (%)	5.2 (37.6)
Refinement statistics	
Resolution range	20–3.4 (3.52–3.40)
R_{free}	32.8 (43.2)
R_{cryst}	26.9 (34.1)
Average B factor (T22-1, T22-2, G8-1, G8-2)	91.4, 116.0, 87.7, 113.6
RMSD from ideality	
Bond lengths (Å)	0.0105
Bond angles (°)	1.80
Ramachandran plot (%) (favored, additional allowed, generously allowed, disallowed)	72.9, 24.3, 2.8, 0

Overall structure. The G8 γδ TCR is composed of four immunoglobulin (Ig) domains: two V domains, which encode the CDR loops, and two C domains, which are assembled into a quaternary structure similar to the previously published human γδ TCR heterodimer (*14*). T22 does not deviate appreciably from the previously described unliganded structure (*11*).

The structure shows that G8 uses its CDR loops to directly contact T22. Thus, the γδ TCR is not interacting with antigen through the germline-encoded framework regions of the V domains, as suggested by some functional studies (*6*, *15*), analogous to superantigen binding to αβ TCR (*16*). Rather, the γδ TCR engages ligand though its predicted antigen binding site. G8 binds T22 at a tilted angle that contrasts with the essentially parallel alignments of the long axes of the αβ TCR and pMHC when in complex (*17*, *18*). The length (12 residues) of the CDR3δ prevents a straight-on approach to T22 that would allow simultaneous close apposition of the CDR1 and CDR2 loops. This results in an almost side-on interaction mode primarily mediated by the δ chain (Figs. 1 and 2). Whereas αβ TCRs and antibodies often use all CDR loops in their recognition of peptide-MHC (pMHC) and protein antigen (Fig. 1, B and C, and Fig. 2) (*4*, *19*), the G8 γδ TCR uses the δ chain as the foundation of the interface with T22, with minor contact by CDR3γ (Figs. 1A and 2). The majority of G8 contact residues are contributed from a CDR3δ loop that binds in a cavity formed by T22's exposed β-sheet platform and α1 helix (Fig. 2).

The G8 γδ TCR interface with T22. The interface between G8 and T22 buries a total of 1936.1 Å^2 of surface area (Fig. 3A), comparable to the buried surface area (BSA) observed in most αβ TCR/pMHC and antibody/antigen interfaces (*19*). G8 contributes 996 Å^2 to the G8/T22 interface, with the overwhelming majority from the Vδ chain (886 Å^2 or

88.9%), and in particular, the CDR3δ (668 Å^2 or 67.1%) (Fig. 3B and table S1). CDR1δ, CDR2δ, HV4δ, and CDR3γ also make small contributions (Fig. 3B and table S1).

The region of buried surface in T22 (940.0 Å^2) is almost entirely within a cavity exposed by the absence of the H1 segment of the α2 helix and bordered by the intact α1 helix and the exposed α1/α2 β sheet (Fig. 3B). This cavity is in a similar location to where classical MHC molecules bind peptide. However, in T22, a 3–amino acid deletion, a disulphide bond between Cys^{110} and Cys^{133}, and the absence of peptide result in a partial unwinding of the α2 helix into a flexible loop (*11*), similar to that seen in the unliganded structure of the human MHC-like molecule, MIC-A (*20*). However, when MIC-A binds to its receptor NKG2D, the disordered segment refolds back into an α helix (*21*). In contrast, G8 binding does not engage the unwound portion of the α2 helix and instead targets the exposed groove (Fig. 3A).

The binding interface of G8's long CDR3δ loop spans from the edge of T22's α1/α2 β-sheet platform to the middle of the β sheet (Fig. 3A). The sideways binding orientation of G8 allows full extension of the CDR3δ loop into this cavity. The CDR3δ BSA is dominated by residues encoded by the two germline Dδ segments used in G8 receptor rearrangement (Fig. 3C), which suggests that the recognition of T22 by γδ TCRs (*10*) is mediated predominantly by restricted components of the CDR3δ loop. The amount of the buried surface area contributed by the CDR3δ loop alone (668 Å^2) is comparable to the entire BSA of some antibody/antigen and αβ TCR/pMHC complexes (table S5).

The bias of CDR3δ in the G8 binding mode contrasts with the majority of known αβ TCR/pMHC and antibody/antigen structure interfaces. There are examples of antibodies that have long CDR3 loops, such as those in the uncomplexed structure of the b12 neutralizing immunoglobulin G antibody against HIV-1 (*22*) and the recent structure of the shark single-domain antibody (IgNAR) in complex with its antigen, lysozyme (*23*). The long CDR3 of the shark IgNAR antibody, instead of extending away from the immunoglobulin domain, is pinned to the core by two disulfide bonds. This constraint reduces the effective length of the CDR loop, resulting in two smaller loops that, combined with the CDR1, compose the binding interface of the IgNAR receptor for lysozyme.

Interface residues. The G8/T22 interface was a well-resolved region of the complex structure, showing clear electron density for the majority of the contacting side chains (Fig. 4A). The CDR3δ loop interacts extensively with the β-sheet platform and truncated α1 helix of T22, undergoing an approximately 180° twist such that the C-terminal region of the loop contacts the α1 helix of T22 while the N-terminal side contacts primarily the β-sheet residues (Fig. 4B). The interface between the CDR loops of G8 and T22 is mediated mostly by hydrophobic interactions, with 84% of T22's contacts and 72% of G8's contacts being apolar residues (table S2 and Fig. 4B).

The primary contact residues in the CDR3δ loop are Thr^{92}, Trp^{93}, Ile^{95}, Gly^{98}, Tyr^{99}, Glu^{100}, and Leu^{101} (Fig. 4B and table S2). Thr^{92} is the result of N-nucleotide addition; Trp^{93} and Ile^{95} are encoded by the second reading frame of the D1 segment; Gly^{98}, Tyr^{99}, and Glu^{100} are encoded by the second reading frame of the D2 segment; and Leu^{101} is the result of P-nucleotide addition. Shin and co-workers have found that the majority of T22 tetramer-positive γδ TCRs characterized have both the Trp^{93} encoded by the germline Dδ1 segment and the repeating motif EGYEL encoded by the Dδ2 segment (*10*). However, they have also observed considerable flexibility in CDR3δ loop length, with G8 having an intermediate length compared with the CDR3δ loops of the T22 tetramer-positive γδ TCRs characterized. Our structure suggests that there are anchor residues in the CDR3δ loop contact interface, in particular Trp^{93} at the N-terminal end of the CDR3 loop, which is part of the extensive aromatic environment on the T22 exposed platform (Fig. 4B) and forms a hydrogen bond with Pro^{124} of T22 (table S3). Residues Gly^{98}, Tyr^{99}, Glu^{100}, Leu^{101}, and Thr^{103} appear to anchor the loop at its C-terminal end, reinforced by three G8/T22 hydrogen bonds (table S3 and Fig. 4B). How T22's cavity can accommodate longer CDR3δ loops in the context of these anchor positions (perhaps additional residues will loop out of the groove) awaits additional structure determinations.

Eight residues in T22 are within van der Waals contact distance to multiple (three or more) residues of G8, which suggests that they are potentially important interactions in the complex interface. Pro^{124} is the most prominent, with six interresidue contacts in the interface (Fig. 4C). Supporting the importance of Pro^{124} in this interface is the finding that an

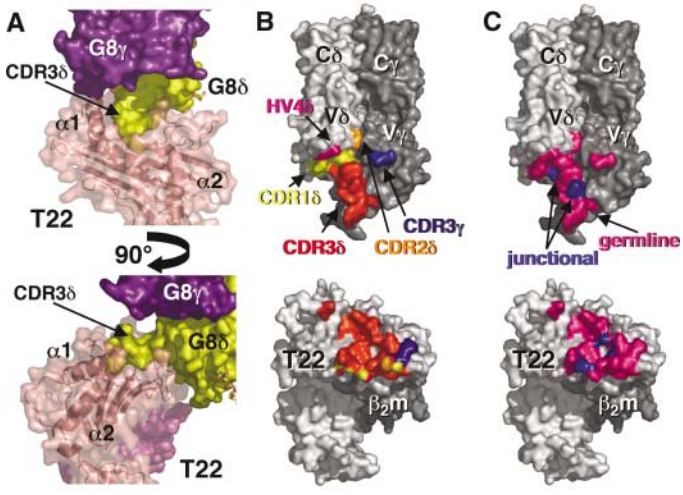

Fig. 3. Distribution of contact surfaces in the interface between the G8 γδ TCR and its MHC ligand T22. (**A**) Shape complementarity between the molecular surfaces of the G8 γδ TCR/T22 interface. The G8 γδ TCR is shown in purple (γ chain) and yellow (δ chain), and the T22 surface (shown in salmon) is transparent to show the ribbon diagram of the α helices and β sheet under it. Much of the interface involves the burying of G8's CDR3δ loop in a cavity over T22's β-sheet platform. (**B**) Breakdown of contacting surfaces between G8 and T22 colored by CDR loop. (Top) The CDR1δ (yellow), CDR2δ (orange), HV4δ (hot pink), and CDR3γ (blue) constitute a minority of the BSA of the G8 γδ TCR interface. The majority of the BSA of the binding interface is contributed by the CDR3δ loop (red). (Bottom) Molecular surface representation of the T22 molecule, with the respective contact sites of the CDR loops mapped onto the surface, color-coded by CDR contact as in the top panel. (**C**) Breakdown of the same contact surface between G8 and T22 colored by germline-encoded (shown in hot pink) versus junctionally generated amino acid residues (blue).

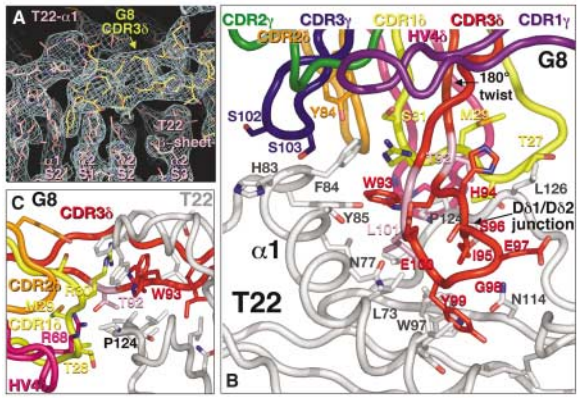

Fig. 4. G8 CDR loop interactions with T22. (**A**) Electron density of the G8/T22 interface showing the insertion of the CDR3δ loop in the T22 cavity (sigmaA-weighted $2F_o$-F_c). (**B**) Contacting amino acid residues within the G8 γδ TCR/T22 interface. The backbone of the CDR3δ loop (shown in red) undergoes a 180° twist. The contact residues of the CDR1δ (yellow), CDR2δ (orange), HV4δ (hot pink), and CDR3γ (blue) loops are also shown. (**C**) Side view showing the central location of the polymorphic T22 residue Pro124 in the G8 interface.

allelic form of the T10 molecule, $T10^d$, does not stimulate G8 (*24*). One of three allelic differences between $T10^d$ and T22 is a histidine instead of a proline at residue 124. This nonconservative substitution likely reduces binding stability and thus inhibits G8 stimulation. One of the Pro^{124} contact residues in the G8 CDR3δ loop, Thr^{92} (Fig. 4C), is encoded by a codon derived from junctional recombination. In other T22 reactive γδ TCRs, the amino acid(s) encoded by this junction vary (*10*), suggesting that the nature of the amino acid at the junction between the V and Dδ1 segment could modulate reactivity between T22 and T10 allelic forms.

Docking flexibility of G8 onto T22. The two G8/T22 complexes in the asymmetric unit have similar contact residues at the interface of the CDR3δ/T22 β sheet. However, extending outward from this interface, the two complexes differ by a relative rotation between the G8 TCRs (~5° rotation for Vδ, ~13° rotation for Vγ), resulting in a translation of approximately 2.4 Å for the δ chain and 6.4 Å for the γ chain when the distances between equivalent carbon-α atoms are measured (Fig. 5) (*13*). This shift alters the contacts formed between CDR1δ, CDR2δ, HV4δ, and CDR3γ loops and T22 in each TCR (table S2 and Fig. 5), suggesting that the CDR3δ loop acts as an anchored pivot point for G8 binding, with some flexibility in the interaction between the other CDR loops and T22.

This binding flexibility between G8 and T22, centered around anchored CDR3δ, is supported by the results of Shin and co-workers (*10*). These results demonstrate promiscuity of Vδ and Vγ chain usage in T22-specific γδ TCRs but conservation of the germline-encoded W…EGYEL motif in the CDR3δ chain. The commonality of this CDR3δ chain motif in T22+ tetramer-stained cells, despite usage of alternate Vδ and Vγ chains, supports the importance of the CDR3δ loop in ligand binding and further suggests that there is degeneracy in the perimeter contacts by the remaining CDR loops to T22. The hingelike flexibility around the pivot point stands in stark contrast to the fixed interactions seen in antibody/antigen and αβ TCR/pMHC complexes. In those cases, the relatively straight-on docking mode results in multipoint (i.e., multi-CDR) attachment of the receptor to the ligand, essentially rigidifying the intermolecular orientations between the two binding partners. In most cases, the αβ TCR CDR1 and CDR2 loops provide a perimeter of contacts with the MHC helices surrounding the CDR3 loops, and so far no variation has been seen in the docking angle of TCR to MHC in cases where multiple complexes exist in the asymmetric unit (*25*, *26*). Thus, the CDR3δ motif of G8 and other γδ TCRs (*10*) may be thought of as a somewhat autonomous binding entity that is presented by a variety of germline-encoded variable domain scaffolds without strong preference for particular CDR1 and 2 sequences.

Dimerization of G8. The two complexes in the asymmetric unit are dimerized through an extensive hydrogen-bonding network that involves the "a" strands of the Vδ domains (Fig. 6 and tables S4 and S5). The orientation of the two TCRs in the asymmetric unit is consistent with a biologically relevant dimer, where the membrane-bound complexes are on opposing cell surfaces. αβ T cells have been shown to require, minimally, oligomerization of their TCRs for activation (*27*); however, there is no crystallographic evidence of biologically relevant αβ TCR dimers. Activation of αβ T cells is also dependent on the expression of appropriate coreceptors such as CD4 or CD8. Some γδ T cells express the CD4 or CD8 coreceptors, yet it is unclear what role they play in γδ T cell activation (*28*). T10/T22–specific γδ T cells, including G8, are $CD4^-/CD8^-$, and therefore their activation appears to be coreceptor independent (*9*).

Dimerization of G8 on the cell surface during ligand binding could circumvent the need for coreceptor involvement and directly facilitate receptor oligomerization and subsequent T cell stimulation (*27*, *29*). However, we have not seen biochemical evidence of oligomerization of the soluble G8 TCR, although the dimerization affinity constant is likely very weak. The high concentration of G8 in the crystallization solution may exceed the dimerization affinity constant in a fashion similar to the elevation in effective concentration achieved by the two-dimensional restriction of the molecules on the cell surface.

Conclusion. The molecular basis of γδ TCR recognition has remained an enigma, as has the immunobiology of γδ T cells. Many characteristics of γδ T cells suggest that they participate early in the immune response, similar to other members of the innate immune system. These features include direct recognition of antigen and immediate effector outcomes such as cytokine release (*30*) and cytotoxicity (*31*). This contrasts with αβ T cells and B cells, both members of the adaptive arm of the immune system, which require a lengthier process of intracellular processing and presentation of antigen for initiation and maintenance of their effector functions. Yet, if γδ TCRs are part of the innate immune system, how do they use their combinatorial diversity in antigen recognition? The structure of G8 γδ TCR in complex with the MHC Ib

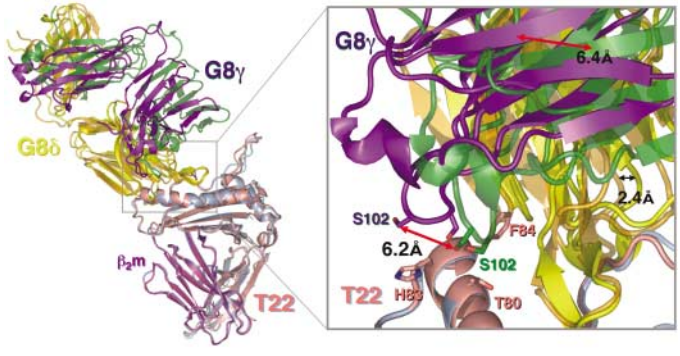

Fig. 5. Hingelike docking flexibility of the G8 TCR on T22. Superimposing the two G8/T22 complexes in the asymmetric unit on the T22 molecules reveals differences in G8 binding orientation centered around the CDR3δ pivot point. (**Left**) The two overall complexes superimposed. Complex 1 is shown as G8 in purple (γ chain) and yellow (δ chain), T22 in salmon (heavy chain) and fuschia (β_2m); complex 2 is shown as G8 in green (γ chain) and orange (δ chain), T22 in light blue (heavy chain) and steel blue (β_2m). (**Right**) Close-up of the Vγ and Vδ domain shifts of the G8 γδ TCR. The cores of the two Vδ domains shift by only 2.4 Å, whereas the two Vγ domains shift by 6.4 Å. For the displacement measurements, the distances between identical TCR residues in the superimposed complexes were measured (*13*).

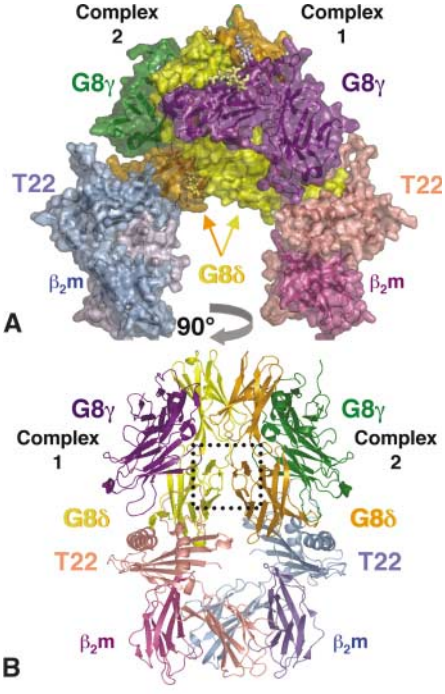

Fig. 6. A dimer of two G8 γδ TCR/T22 complexes. (**A**) Surface representation of the G8/T22 dimer present in the asymmetric unit. Complex 1 shows G8 in purple (γ chain) and yellow (δ chain) complexed to T22 in salmon (heavy chain) and fuschia (β_2m). Complex 2 shows G8 in green (γ chain) and orange (δ chain) complexed to T22 in light blue (heavy chain) and steel blue (β_2m). (**B**) The dimeric interface. The view in (A) is rotated 90° to show the dimer interface along the Vδ domains. The box highlights the location of the two "a" strands involved in the hydrogen-bonding network that constitutes the dimer; see fig. S1 for electron density of this interface.

molecule T22 suggests a convergence of innate and adaptive recognition strategies. G8, like αβ TCRs and antibodies, uses its CDR loops to bind its ligand, T22. However, G8 almost exclusively uses its genetically recombined CDR3δ loop to bind T22 from the side with degenerate contacts for the remaining CDRδ and CDR3γ loops, suggesting that the CDR3δ loop is the primary docking anchor in this recognition strategy. Moreover, the residues involved in the recognition interface are derived predominantly from germline-encoded Dδ segments, suggesting that there is, as previously hypothesized, a germline-encoded basis for T10/T22 recognition. The additional use of junctionally diverse residues in the interface allows for rapid coevolution of γδ TCRs with their ligands. This is an ideal strategy for an innate receptor, because there can be not only a long-term coevolution of the γδ TCR and its ligand over the lifetime of a species but also an immediate fine-tuning of the recognition of its particular ligand within an individual. In this way, the chemistry of the recognition interface between G8 and T22 can be thought of as a hybrid between innate and adaptive recognition solutions.

References and Notes

1. A. C. Hayday, *Annu. Rev. Immunol.* **18**, 975 (2000).
2. Y. H. Chien, R. Jores, M. P. Crowley, *Annu. Rev. Immunol.* **14**, 511 (1996).
3. M. M. Davis, P. J. Bjorkman, *Nature* **334**, 395 (1988).
4. M. G. Rudolph, I. A. Wilson, *Curr. Opin. Immunol.* **14**, 52 (2002).
5. E. P. Rock, P. R. Sibbald, M. M. Davis, Y. H. Chien, *J. Exp. Med.* **179**, 323 (1994).
6. C. T. Morita, R. A. Mariuzza, M. B. Brenner, *Springer Semin. Immunopathol.* **22**, 191 (2000).
7. L. A. Matis, R. Cron, J. A. Bluestone, *Nature* **330**, 262 (1987).
8. H. Schild *et al.*, *Cell* **76**, 29 (1994).
9. M. P. Crowley *et al.*, *Science* **287**, 314 (2000).
10. S. Shin *et al.*, *Science* **308**, 252 (2005).
11. C. Wingren, M. P. Crowley, M. Degano, Y. Chien, I. A. Wilson, *Science* **287**, 310 (2000).
12. M. G. Rudolph, C. Wingren, M. P. Crowley, Y. H. Chien, I. A. Wilson, *Acta Crystallogr. D Biol. Crystallogr.* **60**, 656 (2004).
13. Materials and methods are available as supporting material on *Science* Online.
14. T. J. Allison, C. C. Winter, J. J. Fournie, M. Bonneville, D. N. Garboczi, *Nature* **411**, 820 (2001).
15. S. R. Carding *et al.*, *J. Exp. Med.* **172**, 1225 (1990).
16. E. J. Sundberg, Y. Li, R. A. Mariuzza, *Curr. Opin. Immunol.* **14**, 36 (2002).
17. K. C. Garcia *et al.*, *Science* **274**, 209 (1996).
18. D. N. Garboczi *et al.*, *Nature* **384**, 134 (1996).
19. I. A. Wilson, K. C. Garcia, *Curr. Opin. Struct. Biol.* **7**, 839 (1997).
20. P. Li *et al.*, *Immunity* **10**, 577 (1999).
21. P. Li *et al.*, *Nat. Immunol.* **2**, 443 (2001).
22. E. O. Saphire *et al.*, *Science* **293**, 1155 (2001).
23. R. L. Stanfield, H. Dooley, M. F. Flajnik, I. A. Wilson, *Science* **305**, 1770 (2004).
24. L. A. Matis, J. A. Bluestone, *Semin. Immunol.* **3**, 75 (1991).
25. K. C. Garcia *et al.*, *Science* **279**, 1166 (1998).
26. E. L. Reinherz *et al.*, *Science* **286**, 1913 (1999).
27. Z. Reich *et al.*, *Nature* **387**, 617 (1997).
28. W. Haas, P. Pereira, S. Tonegawa, *Annu. Rev. Immunol.* **11**, 637 (1993).
29. S. M. Hayes, P. E. Love, *Immunity* **16**, 827 (2002).
30. Y. H. Chien, J. Hampl, *Springer Semin. Immunopathol.* **22**, 239 (2000).
31. D. Kabelitz, D. Wesch, *Crit. Rev. Immunol.* **23**, 339 (2003).
32. Y. Li, H. Li, F. Yang, S. J. Smith-Gill, R. A. Mariuzza, *Nat. Struct. Biol.* **10**, 482 (2003).
33. W. L DeLano, DeLano Scientific, San Carlos, CA, USA, 2002.

34. We thank M. Boulanger, P. Strop, and S. Shin for advice and helpful discussions. We also acknowledge Stanford Synchrotron Radiation Laboratory and Advanced Light Source for x-ray resources. This work was supported by a Cancer Research Institute Postdoctoral Fellowship (E.J.A.), an NIH-Immunology postdoctoral training grant (E.J.A), the Keck Foundation, and NIH (AI048540) (K.C.G.). Coordinates of the asymmetric unit have been deposited in the Protein Data Bank with accession code 1YPZ (RCSB031793).

Supporting Online Material

www.sciencemag.org/cgi/content/full/308/5719/227/DC1
Materials and Methods
Fig. S1
Tables S1 to S5

28 October 2004; accepted 9 February 2005
10.1126/science.1106885

REPORTS

The Real-Time Stellar Evolution of Sakurai's Object

Marcin Hajduk,[1,2] Albert A. Zijlstra,[1]* Falk Herwig,[3] Peter A. M. van Hoof,[4,5] Florian Kerber,[6] Stefan Kimeswenger,[7] Don L. Pollacco,[4] Aneurin Evans,[8] José A. Lopéz,[9] Myfanwy Bryce,[10] Stewart P. S. Eyres,[11] Mikako Matsuura[1]

After a hot white dwarf ceases its nuclear burning, its helium may briefly and explosively reignite. This causes the star to evolve back into a cool giant, whereupon it experiences renewed mass ejection before reheating. A reignition event of this kind was observed in 1996 in V4334 Sgr (Sakurai's object). Its temperature decrease was 100 times the predicted rate. To understand its unexpectedly fast evolution, we have developed a model in which convective mixing is strongly suppressed under the influence of flash burning. The model predicts equally rapid reheating of the star. Radio emission from freshly ionized matter now shows that this reheating has begun. Such events may be an important source of carbon and carbonaceous dust in the Galaxy.

Helium-shell flashes play a vital role in the production of chemical elements in stars (*1*). They occur in all stars with initial masses between 1 and 8 times the mass of the Sun, during their asymptotic giant branch (AGB) phase. This phase ends with a drastic and rather sudden episode during which up to 90% of the star's mass is ejected into space. The remnant star evolves through a hot state toward the white dwarf cooling track, where nuclear burning ceases. Its radiation ionizes the ejected material and a planetary nebula forms. About one-quarter of these stars will undergo one final, very late He flash as a white dwarf, after nuclear hydrogen burning has ceased (*1*–*3*), in a unique event of nuclear flash–driven stellar evolution. The reincarnated star retraces its evolution and experiences renewed mass ejection.

The discovery of Sakurai's object (V4334 Sgr) in 1996 provided the first modern observations of this so-called very late thermal pulse (*4*). Its real-time evolution (possibly the fastest ever observed) provides a once-in-a-lifetime observational handle on the physics of convection and rapid nuclear burning. V4334 Sgr was the hot (10^5 K) central star of a hitherto undetected planetary nebula (*5*). Shortly before 1995, the helium layer reignited and V4334 Sgr was reincarnated as a "born-again" giant.

In our Galaxy, such an event is expected to occur once per decade (*6*). But V4334 Sgr was only the third observed case, after V605 Aql in 1918 (*7*) and possibly CK Vul in 1670 (*8*). Other events, such as the eruption of FG Sge (*9*), may have been missed in the crowded regions of the Milky Way. Hydrogen-poor [WC] central stars of planetary nebulae and the cooler hydrogen-deficient and carbon-rich R CrB stars (*10*) may be descendants of the born-again stars.

Computer simulations of the very late He-shell flash show that the small remaining H-rich envelope is convectively ingested into the He shell, resulting in an additional rapid H-driven nuclear flash burning. Initial models predicted that the stellar luminosity would increase, and temperature decrease, over a few hundred years (*1*, *2*). However, V4334 Sgr evolved at 100 times the predicted rate, suggesting neglected physics in the simulations (*11*, *12*). During 1998, increasing opacity by a dusty wind (*13*) rendered V4334 Sgr all but unobservable in the visual region. The mass